

A Confidence-Variance Theory for Pseudo-Label Selection in Semi-Supervised Learning

Jinshi Liu[†], Pan Liu[†]

arXiv:2601.11670v1 [cs.LG] 16 Jan 2026

Abstract—Most pseudo-label selection strategies in semi-supervised learning rely on fixed confidence thresholds, implicitly assuming that prediction confidence reliably indicates correctness. In practice, deep networks are often overconfident: high-confidence predictions can still be wrong, while informative low-confidence samples near decision boundaries are discarded. This paper introduces a Confidence-Variance (CoVar) theory framework that provides a principled joint reliability criterion for pseudo-label selection. Starting from the entropy minimization principle, we derive a reliability measure that combines maximum confidence (MC) with residual-class variance (RCV), which characterizes how probability mass is distributed over non-maximum classes. The derivation shows that reliable pseudo-labels should have both high MC and low RCV, and that the influence of RCV increases as confidence grows, thereby correcting overconfident but unstable predictions. From this perspective, we cast pseudo-label selection as a spectral relaxation problem that maximizes separability in a confidence-variance feature space, and design a threshold-free selection mechanism to distinguish high- from low-reliability predictions. We integrate CoVar as a plug-in module into representative semi-supervised semantic segmentation and image classification methods. Across PASCAL VOC 2012, Cityscapes, CIFAR-10, and Mini-ImageNet with varying label ratios and backbones, it consistently improves over strong baselines, indicating that combining confidence with residual-class variance provides a more reliable basis for pseudo-label selection than fixed confidence thresholds. (Code: https://github.com/ljs11528/CoVar_Pseudo_Label_Selection.git)

Index Terms—Semi-Supervised Learning, Pseudo-Labels, Confidence Calibration, Residual Class Variance, Spectral Relaxation, Semantic Segmentation, Image Classification

I. INTRODUCTION

SEMI-supervised learning (SSL) leverages a small amount of labeled data together with abundant unlabeled data to substantially reduce dependence on manual annotation. Pseudo-labeling, a central paradigm in SSL, derives supervisory signals from the model’s own predictions and has been widely adopted in image classification, semantic segmentation, and text classification[1], [2], [3]. However, most existing methods depend on high-confidence thresholds to select pseudo-labels, assuming a strong correlation between prediction confidence and correctness[4]. This assumption lacks solid theoretical justification and tends to exacerbate the inherent overconfidence of deep models under overfitting. As a result, their predictions tend to cluster in extreme confidence

Jinshi Liu is with the School of Automation, Central South University, Changsha 410083, China. [†] refers to these authors contributed equally to this work. (e-mail: ljs11528@csu.edu.cn)

Pan Liu is with the Information Hub, the Hong Kong University of Science and Technology (Guangzhou), Guangzhou 510006, China. (e-mail: panliu@hkust-gz.edu.cn)

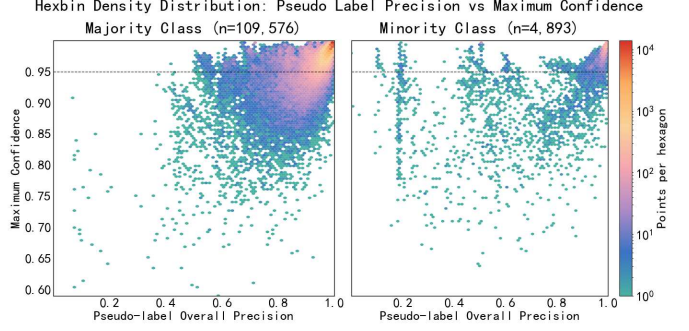


Fig. 1. Relationship between pseudo-label accuracy and maximum confidence on PASCAL VOC 2012 (1/4 split). The sample points in this density plot are collected from the training process spanning epoch 1 to 79. The vertical axis represents the mean of the maximum confidence across all pixels, while the horizontal axis is computed using the validation set. Traditional fixed-threshold methods tend to select a number of low-quality pseudo labels while discarding some high-quality ones (mostly from minority classes), which ultimately leads to suboptimal overall pseudo-label accuracy.

ranges while showing weak correlation with actual accuracy (Fig. 1). Such overconfidence introduces two critical problems:

Confidence Failure. Miscalibration results in correct and incorrect predictions coexisting in high-confidence intervals, undermining confidence reliability;

Degraded Supervision. Low-confidence predictions are systematically discarded, leading to missing supervisory signals in decision boundary regions, hindering discriminative feature learning.

Limited labeled data fails to calibrate the confidence distribution of unlabeled data, severely exacerbating the pseudo-label noise problem. This motivates the need for a principled reliability criterion defined directly on model predictions. Such a criterion should systematically distinguish trustworthy pseudo-labels from unreliable ones. To address this, we propose a unified Confidence-Variance (CoVar) theory framework, which not only leverages joint optimization but also achieves comprehensive coverage over existing threshold-based methods. Our core theoretical contribution is a robust quality assessment criterion that mitigates overconfidence and enhances pseudo-label reliability. Derived from the principle of Entropy Minimization, our analysis reveals that a reliable pseudo-label is defined by the joint optimization of two requirements: sufficiently high Maximum Confidence (MC) and low Residual Class Variance (RCV), which measures the probability mass concentration among non-maximum confidence classes. Crucially, our theoretical derivation exposes a dynamic interaction between these two factors. The negative impact

of a high RCV is dynamically amplified as the prediction's MC increases. This mechanism acts as a penalty, ensuring that any high-confidence prediction is strictly regularized by a correspondingly low RCV to be considered reliable. Reliable predictions, therefore, fundamentally require this joint consideration of both MC and RCV. The main contributions of this paper are:

1) We establish a confidence-variance theory for pseudo-label reliability, deriving a per-sample cross-entropy decomposition into MC and RCV with explicit approximation bounds, a batch-level lower bound, and an adaptive weighting term $g_j(p_j(k'))$ that tightens the RCV penalty as confidence increases.

2) We analyze pseudo-label selection under mini-batch class imbalance, showing that confidence-only rules induce systematic selection bias toward majority classes, and that jointly controlling MC and RCV mitigates this bias and stabilizes pseudo-label coverage across head and tail classes.

3) Guided by this theory, we formulate pseudo-label selection as a spectral relaxation problem in a confidence-variance feature space and derive an efficient solution closely related to kernel spectral clustering, which adaptively separates high- and low-reliability predictions without hand-tuned confidence thresholds and achieves SOTA on multiple semi-supervised segmentation and image classification benchmarks.

II. RELATED WORK

A. Pseudo-Label Selection in Semi-Supervised Learning

Semi-supervised learning [5], [6], [7], [8] leverages both labeled and unlabeled data to improve model generalization. A central challenge in SSL is the selection of reliable pseudo-labels, as naive strategies often suffer from confirmation bias and error accumulation [9], [10], [11], [12], [13]. This has motivated a rich body of work on robust pseudo-label selection mechanisms, ranging from fixed or adaptive confidence thresholds and calibration-based filtering to uncertainty-aware weighting and consistency regularization.

B. Pseudo-Label Selection in Semi-Supervised Image Classification

In semi-supervised image classification, pseudo-label selection is typically based on prediction confidence. Early methods adopt fixed confidence thresholds, while recent works such as FlexMatch [14], FreeMatch [15], and SoftMatch [16] introduce dynamic or adaptive thresholding strategies, or model the confidence distribution to provide more flexible supervision. However, these approaches fundamentally assume that confidence is a reliable proxy for correctness, which is often violated due to model overconfidence. To address this, confidence calibration methods have been introduced as auxiliary mechanisms. Classical post-hoc calibration techniques include temperature scaling [17], Platt scaling [18], and histogram binning [19], while training-time regularization methods such as label smoothing [20], focal loss [21], Mixup [22], and CutMix [23] further mitigate overconfidence. Some works also leverage model uncertainty (e.g., Monte Carlo dropout [24]), ensemble disagreement [25], or auxiliary discriminators [26], but these often introduce significant computational overhead.

C. Pseudo-Label Selection in Semi-Supervised Semantic Segmentation

The challenge of reliable pseudo-label selection is further amplified in semi-supervised semantic segmentation, where pixel-level predictions are required. Early works [27], [1], [28], [29], [30] adapted classification-based SSL frameworks but did not directly address pixel-wise pseudo-label quality. Subsequent research has focused on refining pixel-level selection, including weighting strategies (AEL [31], DAW [32]), multi-hot encoding (ESL [33]), contrastive learning for unreliable predictions (U2PL [34]), and label propagation via correlation maps (CorrMatch [35]). However, the low separability of pixel-wise confidence scores and inherent bias in confidence-based selection remain open problems. Related fields such as unsupervised domain adaptation have also introduced calibration and reliability techniques (TransCal [36], MIC [37]), but fully eliminating bias is still challenging.

In summary, while confidence calibration and alternative selection criteria have advanced pseudo-label selection in both classification and segmentation, most existing methods either remain fundamentally dependent on confidence or incur high computational costs. CoVar instead builds on the entropy minimization principle and shows that reliable predictions require both high confidence and uniform residual-class distributions, a second-order property that is invisible to scalar calibration metrics. This insight enables a theoretically grounded and efficient joint criterion that mitigates confirmation bias and improves pseudo-label discriminability without iterative recalibration or ensemble inference.

III. METHODOLOGY

A. Preliminaries

a) Pseudo-Label Selection in Semi-Supervised Learning:

In semi-supervised learning tasks, the training data consists of a labeled set $D_l = \{(x_i^l, y_i^l)\}_{i=1}^{N_l}$ and an unlabeled set $D_u = \{(x_j^u)\}_{j=1}^{N_u}$, where the number of labeled samples N_l is much smaller than that of unlabeled samples N_u (i.e., $N_l \ll N_u$). The goal of SSL is to learn a model $f_\theta : x \rightarrow y$ that improves performance by simultaneously minimizing a weighted combination of supervised and unsupervised losses:

$$L_s = L_l(D_l) + \lambda L_u(D_u) \quad (1)$$

where $L_u(D_u)$ denotes the unsupervised loss computed on the unlabeled dataset D_u . This loss relies on pseudo-labels \hat{y}_j^u generated by the model for unlabeled samples x_j^u to provide supervisory signals. The coefficient λ serves as a balancing hyperparameter. Meanwhile, $L_l(D_l)$ represents the supervised loss calculated on the labeled dataset D_l , which guides the model to learn discriminative information from known classes.

$$L_l(D_l) = \frac{1}{N_l} \sum_{j=1}^{N_l} \mathcal{L}(y_j^l, f_\theta(x_j^l)) \quad (2)$$

where $\mathcal{L}(\cdot, \cdot)$ denotes the loss function, e.g., cross-entropy (CE). Current confidence-based heuristic pseudo-label selection methods, such as FixMatch [13], primarily employ a confidence threshold mechanism to filter pseudo-labels.

Specifically, for each unlabeled sample x_j^u , the model outputs a predicted class probability distribution $p_j = f_\theta(x_j^u)$, i.e. confidence distribution. If the maximum probability in this distribution exceeds a predefined confidence threshold τ , the class corresponding to this maximum probability is selected as the pseudo-label \hat{y}_j^u ; otherwise, the sample is excluded from the computation of the unsupervised loss.

$$\hat{y}_j^u = \begin{cases} k' & , \text{if } \max(p_{j,k}) \geq \tau \\ \text{ignore} & , \text{otherwise} \end{cases} \quad (3)$$

where $p_j = \{p_j(0), p_j(1), \dots, p_j(k-1)\}$ denotes the confidence distribution, k denotes the number of classes, and $k' = \arg \max_k p_j(k)$ denotes the class with the highest confidence. $\tau \in [0, 1]$ is a predefined fixed threshold whose value may vary across different tasks. Based on this, the unsupervised loss $L_u(D_u)$ is typically constructed by computing the CE between the model prediction p_j and the selected pseudo-label \hat{y}_j^u , incorporated via a loss mask. This mask ensures that only samples satisfying the confidence threshold condition contribute to the unsupervised loss:

$$L_u(D_u) = \frac{1}{N_u} \sum_{j=1}^{N_u} I(\max(p_j(k)) \geq \tau) \cdot \mathcal{L}(\hat{y}_j^u, f_\theta(x_j^u)) \quad (4)$$

where $I(\cdot)$ is an indicator function. This mechanism implicitly relies on the following monotonicity assumption:

Assumption 1 (H_1 : Confidence–accuracy monotonicity). *For any two confidence levels $0 \leq c_1 < c_2 \leq 1$,*

$$\mathbb{P}(\hat{y}_j^u = y_j^u \mid C_j = c_1) < \mathbb{P}(\hat{y}_j^u = y_j^u \mid C_j = c_2), \quad (5)$$

where $C_j = \max_k p_j(k)$ is the maximum predicted confidence and $\mathbb{P}(\hat{y}_j^u = y_j^u)$ denotes the probability that the pseudo-label \hat{y}_j^u matches the true label y_j^u .

b) Theoretical Limitations of the Fixed Threshold Method: The vast majority of existing state-of-the-art (SOTA) semi-supervised learning methods adopt a fixed confidence threshold. However, some researchers have observed that assumption H_1 may fail in deep learning models (Fig. 2), which manifests itself in two aspects:

1) *Overconfidence decouples confidence from accuracy:* We measure the mismatch between confidence and accuracy by the Expected Calibration Error (ECE):

$$\text{ECE} = \mathbb{E}_{x \sim D_u} [|\mathbb{P}(\hat{y} = y \mid \max(p) = \tau) - \tau|], \quad (6)$$

where τ is the confidence level used for binning. Prior work has shown a persistent confidence-accuracy gap $\Delta = |\mathbb{P}(\hat{y} = y \mid \max(p) = \tau) - \tau| > 0$ [38]. Fig. 2 further confirms this in our SSL setting: the pseudo-label accuracy curve $a(\tau)$ is consistently below the ideal line $y = \tau$ for $\tau \in [0.90, 0.99]$, revealing that fixed-threshold methods are inherently overconfident on high-confidence pseudo labels.

2) *Class imbalance in mini-batch training amplifies this bias:* Consider a mini-batch $B = \{x_i\}_{i=1}^{N_B}$ and its class-specific subset $B_k = \{x \in B \mid y = k\}$. Under a fixed threshold, the retention rate of pseudo labels from class k can be written as

$$r_k = \frac{|\{x \in B_k \mid \max(p) \geq \tau\}|}{|B_k|} \leq \frac{A}{\sqrt{N_k}}, \quad (7)$$

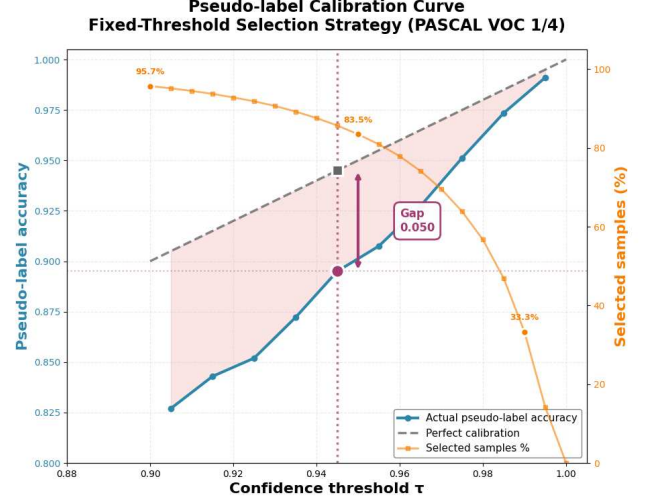


Fig. 2. Pseudo-label accuracy and selection ratio under different confidence thresholds on PASCAL VOC 1/4. The blue curve shows the pseudo-label accuracy $a(\tau) = \mathbb{P}(\hat{y} = y \mid \max(p) \geq \tau)$ under a fixed-threshold selection strategy, while the orange curve indicates the proportion of samples whose maximum confidence exceeds τ . The gray dashed line represents the ideal calibration $y = \tau$; the gap at a typical threshold (e.g., $\tau_0 = 0.95$) visualizes the calibration error $\Delta = |\mathbb{P}(\hat{y} = y \mid \max(p) \geq \tau_0) - \tau_0|$. The gap further highlights that high-confidence predictions are systematically overconfident, revealing an inherent mismatch between confidence and true accuracy in fixed-threshold methods.

where A is a task-dependent constant and N_k denotes the number of samples from class k . This implies that minority classes (with smaller N_k) suffer from a much lower retention rate, while majority classes are more likely to be preserved as pseudo labels. As shown by the orange curve in Fig. 3, increasing the confidence threshold rapidly reduces the proportion of selected samples, which further amplifies the imbalance between majority and minority classes and makes performance highly sensitive to the choice of τ .

B. Confidence-Variance Theoretical Framework

a) *Pseudo-Label Selection at the Sample Level:* Entropy minimization is one of the core strategies in semi-supervised learning, aimed at improving model performance by reducing prediction uncertainty on unlabeled data. The central idea is to encourage the model to make high-confidence predictions for unlabeled samples, thereby pushing the decision boundary away from high-density data regions. After predicting on unlabeled data, samples with high confidence (low entropy) are selected to generate pseudo-labels, which are then incorporated into the training set for iterative optimization. Entropy minimization is typically incorporated as an additional unsupervised term in the training objective and optimized jointly with the supervised loss, acting as a regularizer that encourages low-entropy predictions on unlabeled data.

Consider a batch B containing N_B unlabeled samples and their prediction results, where p_j denotes the confidence (probability) distribution for the j -th sample. Let $p_j(k')$ be the MC value and $k' = \arg \max_k p_j(k)$ be the class corresponding to this maximum value. Under the principle of entropy mini-

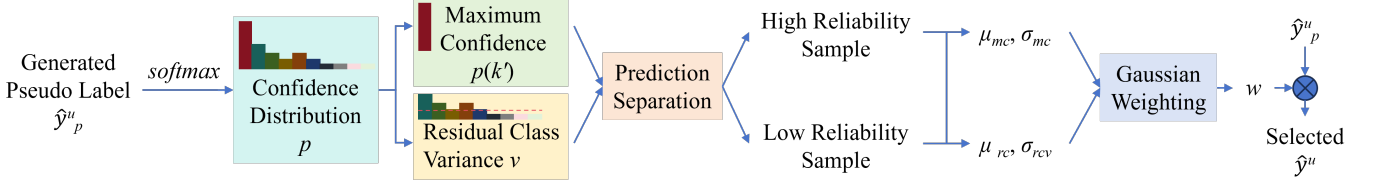


Fig. 3. The overall pipeline of the proposed method. Based on the proposed confidence-variance theory, the prediction separation module divides pseudo labels into high-reliability and low-reliability groups. Then, Gaussian weighting is applied to transform the statistical characteristics of MC and RCV into pseudo-label weights, enabling the selection of high-quality pseudo labels.

mization, an ideal confidence distribution for a sample can be represented as

$$q(k) = \begin{cases} 1 - (K-1)\varepsilon & \text{if } k = k' \\ \varepsilon & \text{if } k \neq k' \end{cases} \quad (8)$$

where the confidence values of non-maximum classes $\varepsilon \rightarrow 0$ and K is the number of classes. In practice, entropy minimization is usually implemented via a CE surrogate between the model prediction p_j and such an ideal target distribution q_j . The CE for a single sample can then be written as

$$CE(p_j, q_j) = -q_j(k') \log p_j(k') - \varepsilon \sum_{k \neq k'} \log p_j(k). \quad (9)$$

For each sample j and every non-maximum class $k \neq k'$, let $\mu_j = \frac{1-p_j(k')}{K-1}$ and $\delta_j(k) = p_j(k) - \mu_j$ with $\sum_{k \neq k'} \delta_j(k) = 0$. Assume there exists $\rho \in (0, 1)$ such that $|\delta_j(k)| \leq \rho \mu_j$ for all $k \neq k'$. Equivalently, all residual-class probabilities satisfy $p_j(k) \in [(1-\rho)\mu_j, (1+\rho)\mu_j] \subset (0, 1)$. Then, performing a second-order Taylor expansion of $\log p_j(k)$ at $p_j(k) = \mu_j$:

$$\log p_j(k) = \log \mu_j + \frac{\delta_j(k)}{\mu_j} - \frac{\delta_j^2(k)}{2\mu_j^2} + R_2(p_j(k)) \quad (10)$$

Substituting Eq. 10 into Eq. 9 above gives:

$$\begin{aligned} CE(p_j, q_j) &\approx -\log p_j(k') - (K-1)\varepsilon \log \frac{p_j(k')}{1-p_j(k')} \\ &\quad + \frac{(K-1)^3 \varepsilon}{2(1-p_j(k'))^2} \cdot v_j \\ &= -f_j(p_j(k')) + g_j(p_j(k')) \cdot v_j \end{aligned} \quad (11)$$

where both $f_j(p_j(k')) = \log p_j(k') + (K-1)\varepsilon \log \frac{p_j(k')}{1-p_j(k')}$ and $g_j(p_j(k')) = \frac{(K-1)^3 \varepsilon}{2(1-p_j(k'))^2}$ are monotonically increasing functions with respect to $p_j(k')$, and the RCV v_j is:

$$v_j \triangleq \frac{1}{K-1} \sum_{k \neq k'} \delta_j^2(k) \quad (12)$$

This result indicates that, under the entropy minimization objective, a reliable prediction requires simultaneously maximizing the $p_j(k')$ and minimizing the v_j . Notably, as $p_j(k') \rightarrow 1$, the coefficient term $g_j(p_j(k'))$ of v_j becomes significant, suggesting that v_j serves as an important indicator for distinguishing prediction reliability in overconfident scenarios. The detailed derivations and theoretical proofs of Eq. 9–12 can be found in the supplementary material.

b) Pseudo-Label Selection at Batch Level: In the single-sample case (batch size = 1), Eqs. 9–12 provide a local approximation in terms of the maximum confidence $p_j(k')$ and the residual-class variance v_j , showing that “high MC + low RCV” is a necessary condition for a reliable prediction. However, in practical training the model is almost always updated on mini-batches with $N_B \gg 1$, and naively applying this single-sample rule to each element of a batch has two important limitations.

First, from a theoretical perspective, the per-sample CE enters the analysis only through an approximation that depends on the ideal target distribution q_j and higher-order residual terms R_j , rather than as a stable closed-form function of $(p_j(k'), v_j)$. Different samples (especially from different classes) have different ideal confidence profiles. Treating this approximation as an exact per-sample score and ranking or truncating samples within a batch therefore amplifies approximation errors.

Second, a mini-batch is a random subset drawn from a long-tailed data distribution. Samples from different classes exhibit markedly different batch-normalization statistics and confidence distributions, and the counts of majority and minority classes are often highly unbalanced. Under such conditions, independent per-sample scoring remains essentially equivalent to a more refined fixed-threshold or top- K rule: high-confidence majority-class samples dominate pseudo-label selection, while reliable minority-class pseudo-labels are systematically underselected. In other words, a purely single-sample view cannot capture the overall inter-class structure and selection bias within a batch.

1) Setting the Ideal Residual-Class Confidence ε : As discussed above, we fit the model’s predictive distribution p_j to an almost one-hot ideal distribution q , whose residual-class mean is an infinitesimal ε . In practice, however, the residual-class mean of the model prediction, denoted by μ_j , almost never equals zero [39]. Consequently, the CE numerically mixes two sources of error: (i) the discrepancy in the total amount of residual-class confidence, and (ii) the discrepancy in how this residual mass is distributed across classes (i.e., its variance). Since concrete numerical values must be used in computation and ε would otherwise vary across samples and classes, we set ε in the ideal distribution q equal to the residual-class mean of the model prediction itself, i.e., $\varepsilon = \mu_j = \frac{1-p_j(k')}{K-1}$. Combined with Eq. 12, this yields the simplified form adopted in Eq. 13.

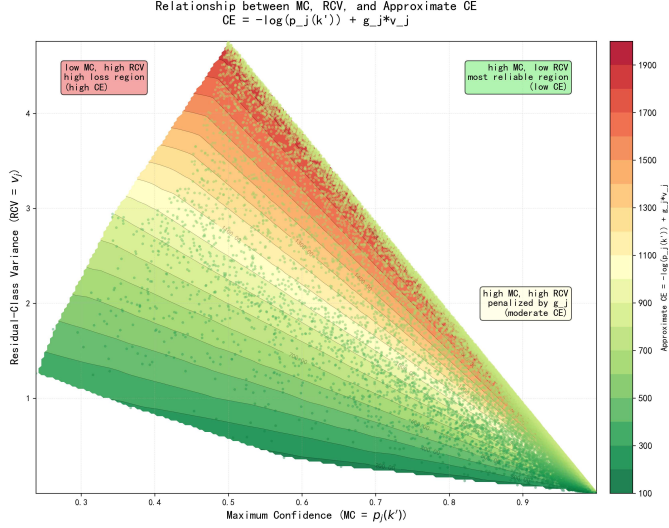


Fig. 4. Illustration of the approximate CE loss $CE = -\log(p_j(k')) + \frac{(K-1)^2}{2(1-p_j(k'))} v_j$ on the plane spanned by model confidence $p_j(k')$ and relative confidence variation v_j . The contour map shows that (i) samples with low confidence and large variation (top-left region) incur very high loss, (ii) even high-confidence predictions with large variation (top-right region) are heavily penalized due to the large gradient factor g_j , and (iii) the most reliable pseudo-labeled samples concentrate in the high-confidence, low-variation region (bottom-right), where the loss remains minimal.

The batch CE can then be expressed as:

$$\begin{aligned}
 CE_B &= \frac{1}{N_B} \sum_{j=1}^{N_B} CE(p_j, q_j) \\
 &\approx \frac{1}{N_B} \sum_{j=1}^{N_B} \left(-\log p_j(k') + (K-1)\varepsilon \log \frac{1-p_j(k')}{p_j(k')} \right. \\
 &\quad \left. + \frac{(K-1)^3 \varepsilon}{2(1-p_j(k'))^2} \cdot v_j \right) \\
 &= \frac{1}{N_B} \sum_{j=1}^{N_B} \left(-\log p_j(k') + \frac{(K-1)^2}{2(1-p_j(k'))} \cdot v_j \right) \\
 &\quad + \frac{1}{N_B} KL \left(\frac{1-p_j(k')}{p_j(k')} \right) \\
 &\geq \frac{1}{N_B} \sum_{j=1}^{N_B} \left(-\log p_j(k') + \frac{(K-1)^2}{2(1-p_j(k'))} \cdot v_j \right)
 \end{aligned} \tag{13}$$

This choice means that we no longer measure the distance between p_j and an abstract one-hot vector, but rather, under a fixed total residual confidence $(1 - p_j(k'))$, we measure how far the allocation of residual-class confidence deviates from the most ideal allocation, namely a uniform distribution (see Fig. 4). As a result, the loss component due to the total residual mass is decoupled from the component determined by its distributional shape. The latter is precisely captured by v_j , allowing the variance term to quantify fluctuations over residual classes in a way that is not confounded by the total residual mass. Crucially, the resulting lower bound is entirely determined by the prediction p_j itself, thereby exhibiting a sample-adaptive characteristic.

2) Batch-Level Decomposition and Inter-Class Effects:

The limitations of the single-sample view motivate a direct analysis at the batch level. By rewriting the average batch CE in terms of MC and RCV statistics, we obtain the three-term decomposition in Eq. 14:

$$\begin{aligned}
 CE_B &= \frac{1}{N_B} \sum_{j=1}^{N_B} CE(p_j, q_j) \\
 &\approx \frac{1}{N_B} \sum_{j=1}^{N_B} \left(-f_j(p_j(k')) + g_j(p_j(k')) \cdot v_j \right) \\
 &= -\frac{1}{N_B} \sum_{j=1}^{N_B} f_j(p_j(k')) + \frac{1}{N_B} \sum_{j=1}^{N_B} (g_j(p_j(k')) \cdot v_j) \\
 &= -\underbrace{\frac{1}{N_B} \sum_{j=1}^{N_B} f_j(p_j(k'))}_{\bar{MC}} + \underbrace{\bar{g} \cdot \bar{v}}_{s\bar{RCV}} + \underbrace{\text{Cov}(g, v)}_{\text{Sample Consistency}}
 \end{aligned} \tag{14}$$

where $\bar{g} = \frac{1}{N_B} \sum_j g_j(p_j(k'))$, $\bar{v} = \frac{1}{N_B} \sum_j v_j$, and $\text{Cov}(g, v) = \frac{1}{N_B} \sum_j (g_j(p_j(k')) - \bar{g})(v_j - \bar{v})$.

\bar{MC} is the batch mean of the negative log maximum confidence, $s\bar{RCV} = \bar{g} \bar{v}$ is the scaled average residual-class variance, and $\text{Cov}(g, v)$ is the covariance between $g_j(p_j(k'))$ and v_j within the batch. This decomposition acts directly on the batch objective, rather than serving as an independent per-sample scoring rule, and allows us to explicitly analyze three factors: (i) the gain in overall confidence through \bar{MC} ; (ii) the suppression of overconfidence by reducing the mean residual variance \bar{v} in $s\bar{RCV}$; and (iii) the role of $\text{Cov}(g, v)$ in measuring whether high confidence co-occurs with well-behaved residual distributions, thereby explaining and mitigating systematic majority-class bias in pseudo-label selection. Compared with heuristic single-sample thresholds, this batch-level formulation preserves the MC/RCV structure of the single-sample theory while explicitly modeling inter-class differences and long-tail imbalance via the covariance term, yielding a tractable batch-wise pseudo-label selection scheme aligned with the training objective.

C. Prediction Separation via Spectral Relaxation

Building on Lemma 1 and Theorem 1 (see the supplementary material), the single-sample analysis shows that reliability is governed jointly by the maximum confidence $p_j(k')$ and the residual-class variance v_j , with an adaptive penalty on v_j that increases with $p_j(k')$ (cf. Theorem 2 at the batch level). This induces a nonlinear coupling between confidence and variance that fixed-threshold rules (on either confidence or entropy) cannot capture, so we formulate pseudo-label selection as a partitioning problem in a confidence-variance feature space with theoretically motivated, confidence-aware scaling, and solve it via spectral relaxation to obtain a tractable surrogate that separates high- and low-reliability predictions while adhering to the joint MC/RCV criterion (Fig. 3).

As discussed in Section 3.2, the reliability of a prediction depends nonlinearly on $p_j(k')$ and v_j . Conventional fixed-threshold methods fail to capture the nonlinear and comple-

mentary relationship between these two factors. To address this limitation, guided by our theoretical framework, we reformulate pseudo-label selection as a spectral partitioning problem in the feature space. The objective is to divide the predictions into two subsets, corresponding to high- and low-reliability samples, by jointly considering $p_j(k')$ and v_j .

a) *Attribute Embedding and Problem Formulation:* For each prediction unit (which can be a pixel, a region, or any task-dependent unit of prediction), an initial attribute vector is constructed: $\mathbf{h}_j = [p_j(k'), -v_j]^T$. This form assumes equal importance of both attributes; however, our theoretical analysis reveals that their contributions to prediction reliability are asymmetric. In particular, under the entropy minimization objective, the coefficient of v_j increases significantly as $p_j(k') \rightarrow 1$. To capture this imbalance, we introduce a weight vector $W = [\alpha, \beta]^T$, where $\alpha, \beta > 0$, and redefine the attribute embedding as:

$$\tilde{\mathbf{h}}_j = W \cdot \mathbf{h}_j = [\alpha \cdot \log p_j(k'), -\beta \cdot v_j]^T \quad (15)$$

where W is a diagonal weighting matrix. Based on our earlier derivation (Eq. 13), the coefficient of v_j is $-\frac{(K-1)^2}{2(1-p_j(k'))}$, which is a monotonically increasing function. We therefore redefine the attribute embedding as:

$$\tilde{\mathbf{h}}_j = W \cdot \mathbf{h}_j = [\log p_j(k'), -\frac{(K-1)^2}{2(1-p_j(k'))} \cdot v_j]^T \quad (16)$$

This mapping introduces confidence-aware nonlinear scaling that projects predictions into a feature space compatible with spectral relaxation. The similarity matrix $\Phi^T \Phi$ implicitly encodes a kernelized representation where the adaptive weighting functions as a task-dependent kernel. Thus, the method extends spectral clustering to adaptively weight MC and RCV according to their theoretical impact on prediction reliability, partitioning predictions into high- and low-reliability subsets without hand-tuned thresholds.

Our goal is to partition these embeddings into two clusters such that predictions with both high MC and low RCV are grouped together. This can be formalized as a trace maximization objective:

$$\max_{\mathbf{S}} \text{Tr}(\mathbf{S}^T \Phi^T \Phi \mathbf{S}), \quad \text{s.t. } \mathbf{S} \in \{0, 1\}^{N \times 2} \sum_c S_{n,c} = 1 \quad (17)$$

where $\text{Tr}(\cdot)$ denotes the matrix trace, $\Phi = [\mathbf{h}_1, \mathbf{h}_2, \dots, \mathbf{h}_N]$ is the feature matrix of all predictions, and \mathbf{S} is the cluster assignment matrix subject to the constraint that each row has exactly one nonzero entry (equal to 1).

b) *Spectral Relaxation and Solution:* The combinatorial optimization problem above is NP-hard. Drawing on the spectral clustering framework [40], we relax the discrete constraints into a continuous form via spectral relaxation. According to the Ky Fan theorem [41], the optimal solution can be approximated using the first two eigenvectors of the similarity matrix $\Phi^T \Phi$. The relaxed assignment rule is:

$$S_{n,c}^* = \Delta(\arg \max_{i \in \{1, 2\}} |u_i(n)|, c) \quad (18)$$

where u_1, u_2 are the eigenvectors of $\Phi^T \Phi$, $|u_c(j)|$ denotes the absolute value of the j -th element of u_c , and $\Delta(\cdot, \cdot)$ is the

Kronecker delta function. Intuitively, this assigns each prediction to the cluster corresponding to the dominant component in the eigenvector representation.

c) *Projection and Weight Construction:* Let $c = 2$ denote the high-reliability cluster. We define a projection matrix $Z = \Phi S_{:,2}^*$, which maps predictions to their reliable components. Then, smooth loss weights are constructed using a Gaussian weighting function:

$$\omega_n = \prod_c \exp \left(\frac{(\tilde{h}_n(c) - \mu_c)^2}{-2\sigma_c^2} \right) \quad (19)$$

where μ_c and σ_c are the mean and variance of the reliable predictions in the projected space along dimension c . For predictions identified as highly reliable, the weight is fixed to 1. Finally, the task-dependent indicator mapping M_i is:

$$M_i(n) = \begin{cases} 1 & \text{if } (\tilde{h}_n(c) - \mu_c) > 0, \forall c \in \{1, 2\}, \\ \omega_n & \text{Otherwise.} \end{cases} \quad (20)$$

This method effectively distinguishes reliable from unreliable predictions based on the joint feature distribution of confidence and dispersion. It is general and applicable to arbitrary classification tasks.

IV. EXPERIMENTS

A. Datasets and Experimental Setup

a) *Datasets:* We evaluated the proposed method on two representative tasks: semi-supervised semantic segmentation and semi-supervised image classification.

Semantic Segmentation. Experiments were conducted on two benchmark datasets, PASCAL VOC 2012 and Cityscapes[42], [43]. PASCAL VOC 2012 is a standard dataset containing 20 object categories and one background class, with 1,464 images for training and 1,449 for validation. Following common practice, the training set was augmented with 9,118 additional images from the Segmentation Boundary Dataset[44], resulting in a total of 10,582 training images. Cityscapes focuses on urban scene understanding and includes 19 categories, comprising 2,975 finely annotated training images and 500 validation images at a resolution of 1024×2048 .

Image Classification. For semi-supervised image classification, we evaluated our method on CIFAR-10 and Mini-ImageNet[45], [46]. CIFAR-10 consists of 10 classes with 60,000 color images of size 32×32 , including 50,000 for training and 10,000 for testing. Following the standard semi-supervised protocol, a small subset of the training images was randomly selected as labeled data, with the remainder treated as unlabeled. Mini-ImageNet is a commonly used subset of ImageNet containing 100 classes, each with 600 color images of size 84×84 (500 for training and 100 for testing). Under the semi-supervised setting, we similarly partitioned the training set into labeled and unlabeled portions to evaluate performance under limited annotation.

b) *Implementation Details:* For semi-supervised semantic segmentation, we compared our method with two representative SOTA baselines: CSL (ResNet-101 backbone) and UniMatchV2 (Transformer backbone). All experiments used stochastic gradient descent with a batch size of 8 and a

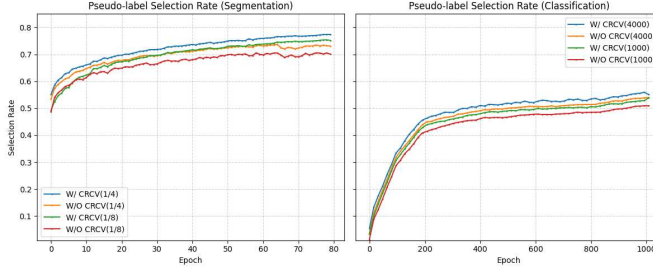


Fig. 5. Change in pseudo-label selection rate during different model training processes. Experiments are conducted on the blender PASCAL VOC 2012 (321×321) and CIFAR-10. Compared to the fixed threshold method, our approach can significantly improve the pseudo-label selection rate.

weight decay of 1×10^{-4} . For PASCAL VOC 2012, the initial learning rate was 0.001, crop sizes were set to 321×321 or 513×513 , and training was performed for 80 epochs. The decoder learning rate was set to 10 times that of the backbone. For Cityscapes, we used the same initial learning rate with a crop size of 801×801 , trained for 240 epochs, and adopted the Online Hard Example Mining loss for fair comparison.

For semi-supervised image classification, we used SimPLE as the baseline, a SOTA method built on the Wide ResNet-28-2 architecture. Optimization employed AdamW with weight decay, and exponential moving average (EMA) was applied to model parameters for evaluation and label prediction. Unless otherwise specified, the confidence threshold was fixed at $\tau_c = 0.95$ and the EMA decay rate at 0.999.

c) Evaluation Metrics and Environment: For the PASCAL VOC 2012 dataset, we follow standard evaluation protocols used in previous studies, report the mean Intersection over Union (mIoU) calculated on the original validation images. For the Cityscapes dataset, consistent with prior approaches, we perform sliding window evaluation with a crop size of 801×801 and compute the mIoU. All results are measured on the standard validation sets of PASCAL VOC 2012 and Cityscapes. Ablation studies are conducted on the original PASCAL VOC 2012 datasets with a crop size of 321×321 .

B. Performance Improvement When Integrated with Existing SOTA Methods

To validate the versatility and effectiveness of the proposed framework, we evaluated it on two representative semi-supervised tasks: semantic segmentation and image classification. For semantic segmentation, we adopt UniMatch as the base framework and augment it with CoVar, while for image classification we build on SimPLE and equip it with the CoVar. For each setting, we compared against the corresponding baseline under multiple label partitions to assess performance changes in a broad and robust manner.

Semi-Supervised Semantic Segmentation: On both the original and augmented PASCAL VOC 2012 and Cityscapes benchmarks, CoVar yields consistent mIoU gains over strong baselines across all label ratios (Table I, II). On VOC 321×321 (1/16 split), it improves ST++ / UniMatch / CorrMatch / CSL by +3.7 / +1.7 / +0.6 / +0.4 mIoU and still surpasses CorrMatch (+1.0) and CSL (+0.3) at 1/4; at 513×513 , CoVar

TABLE I
COMPARISON WITH SOTAS ON PASCAL VOC 2012 BLENDER DATASET

PASCAL blender	Backbone	Train Size	1/16*	1/8*	1/4*
ST++ [47]	ResNet-101	321×321	74.5	76.3	76.6
UniMatch V1 [29]	ResNet-101	321×321	76.5	77.0	77.2
CorrMatch [35]	ResNet-101	321×321	77.6	77.8	78.3
CAC [48]	ResNet-101	321×321	72.4	74.6	76.3
CSL [8]	ResNet-101	321×321	77.8	78.5	79.0
CoVar (Ours)	ResNet-101	321×321	78.2	78.7	79.3
ST++ [47]	ResNet-101	513×513	74.7	77.9	77.9
UniMatch V1 [29]	CLIP-B	513×513	78.1	78.4	79.2
CorrMatch [35]	ResNet-101	513×513	78.4	79.3	79.6
ESL [33]	ResNet-101	513×513	76.4	78.6	79.0
PS-MT [28]	ResNet-101	513×513	75.5	78.2	78.7
CFCG [49]	ResNet-101	513×513	76.8	79.1	80.0
CCVC [50]	ResNet-101	513×513	77.2	78.4	79.0
DLG [51]	ResNet-101	513×513	77.8	79.3	79.1
RankMatch [52]	ResNet-101	513×513	78.9	79.2	80.0
DGCL [53]	ResNet-101	513×513	76.6	78.3	79.3
AllSpark [54]	MiT-B5	513×513	78.3	80.0	80.4
DDFP [55]	ResNet-101	513×513	78.3	78.9	79.8
CSL [8]	ResNet-101	513×513	78.9	79.9	80.3
UniMatch V2 [1]	DINOv2-B	513×513	<u>85.3</u>	<u>87.9</u>	<u>88.8</u>
CoVar (Ours)	ResNet-101	513×513	79.2	80.4	80.4
CoVar (Ours)	DINOv2-B	513×513	86.6	89.1	89.9
U2PL [†] [34]	ResNet-101	513×513	77.2	79.0	79.3
GTA [†] [56]	ResNet-101	513×513	77.8	80.4	80.5
CorrMatch [†] [35]	ResNet-101	513×513	81.3	81.9	80.9
UniMatch V1 [†] [29]	CLIP-B	513×513	81.0	81.9	80.4
AugSeg [†] [57]	ResNet-101	513×513	79.3	81.5	80.5
AllSpark [†] [54]	MiT-B5	513×513	<u>81.6</u>	82.0	80.9
CSL [†] [8]	ResNet-101	513×513	81.6	82.4	<u>81.1</u>
CoVar (Ours) [†]	ResNet-101	513×513	81.7	82.6	81.4

* All labelled images were selected from the blender VOC training set under different splits, which consists of 10,582 images. [†] means using U2PL's splits.

TABLE II
COMPARISON WITH SOTAs ON CITYSCAPES DATASET

Cityscapes	Backbone	1/16(186)	1/8(732)	1/4(744)	1/2(1488)
Supervised	ResNet-101	63.1	70.5	73.1	76.2
ST++ [47]	ResNet-101	67.6	73.4	74.6	77.8
UniMatch V1 [29]	CLIP-B	76.6	77.9	79.2	79.5
CorrMatch [35]	ResNet-101	77.3	78.5	79.4	80.4
ESL [33]	ResNet-101	75.1	77.2	79.0	80.5
DGCL [53]	ResNet-101	73.2	77.3	78.5	80.7
AugSeg [57]	ResNet-101	75.2	77.8	79.6	80.4
CCVC [50]	ResNet-101	74.9	76.4	77.3	-
DAW [32]	ResNet-101	76.6	78.4	79.8	80.6
U2PL [34]	ResNet-101	70.3	74.4	76.5	79.1
CPS [58]	ResNet-101	69.8	74.3	74.6	76.8
DDFP [55]	ResNet-101	77.1	78.2	79.9	80.8
SemiVL [59]	CLIP-B	72.2	75.4	77.2	79.6
FPL [60]	ResNet-101	75.7	78.5	79.2	-
AllSpark [54]	MiT-B5	78.3	79.2	80.6	81.4
CSL [8]	ResNet-101	78.2	78.8	80.0	81.1
UniMatch V2 [1]	DINOv2-B	<u>82.6</u>	<u>83.3</u>	<u>83.5</u>	<u>84.1</u>
CoVar (Ours)	ResNet-101	78.3	78.6	80.1	81.3
CoVar (Ours)	DINOv2-B	83.7	84.4	85.0	85.3

* All methods are built upon DeepLabV3+ [61] and ResNet101 [62].

reaches 79.2-80.4 mIoU with ResNet-101 and 86.6 / 89.1 / 89.9 mIoU (1/16 / 1/8 / 1/4) with DINOv2-B, exceeding UniMatch V2 by +1.3 / +1.2 / +1.1. Under the U2PL protocol, CoVar (81.7) marginally outperforms CSL (81.6), indicating that as representational quality improves, the adaptive coupling

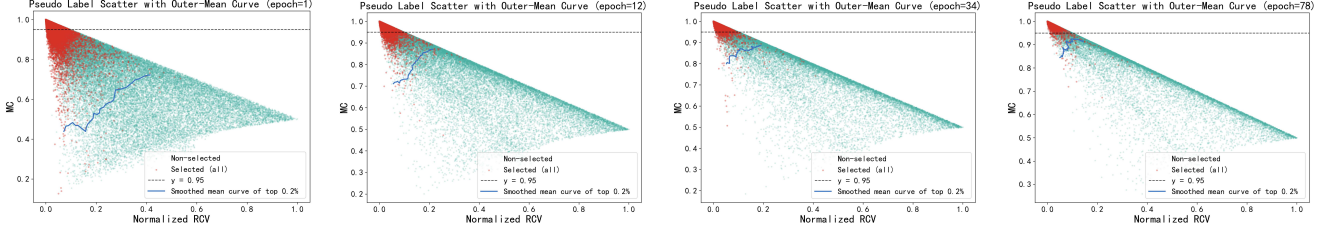


Fig. 6. The variation of the sample’s MC and RCV during model training. Experiments are conducted on the blender PASCAL VOC 2012 dataset (1/4, 321x321, 100,000 sample points are randomly sampled in each epoch). The fixed-threshold method selects only those sample points with $MC > 0.95$. As training progresses, our pseudo-label selection strategy tends to choose more reliable pseudo-labels (those with high MC and low RCV in the remaining classes), rather than relying solely on MC for selection.

of maximum confidence and residual-class variance continues to provide additive regularization.

On Cityscapes (Table. II), gains are most pronounced in low-label regimes: with DINOv2-B, CoVar improves over Uni-Match V2 by +1.1 / +1.1 / +1.5 / +1.2 mIoU at 1/16 / 1/8 / 1/4 / 1/2. Comparing ResNet-101 vs. DINOv2-B shows backbone strength lifts the performance floor but does not eliminate CoVar’s margin, evidencing that joint MC-RCV screening suppresses overconfident majority-class drift and long-tail bias even in high-quality feature spaces. Across ResNet-101, CLIP-B, MiT-B5, and DINOv2-B, CoVar’s absolute improvements remain stable in the mid-high accuracy band and shift from broad confidence filtering to fine-grained residual distribution calibration when the backbone is very strong.

Semi-Supervised Image Classification: On CIFAR-10 (Table. III), where performance is near saturation, CoVar attains 95.60% at 4000 labels (tying FlexMatch, -0.02 below FreeMatch) and improves SimPLE by +0.65 (4000 labels) and +0.15 (1000 labels), indicating residual dispersion filtering still yields incremental refinement under low noise. On Mini-ImageNet, larger class granularity amplifies its effect: +2.09 (WRN-28-2, SimPLE→CoVar) and +3.21 (ResNet-18, SimPLE→CoVar), and +9.26 over Enhanced MixMatch (ResNet-18). Stronger backbones (ResNet-18 vs. WRN-28-2) convert reliability screening into larger boundary shifts; on CIFAR-10 the gain compresses because high-confidence errors are already scarce. This mirrors segmentation: improvements stem from discriminating high-confidence but uneven residual distributions rather than replacing simple thresholds.

Across segmentation and classification, CoVar’s adaptive confidence-variance weighting consistently translates theoretical reliability conditions into practical selection gains that are largely independent of backbone family. Even strong encoders gain from CoVar: by tightening residual-class uniformity on near-certain predictions, it delivers higher pseudo-label selection rates than fixed thresholds across training (Fig. 5), working as a plug-and-play reliability module under varied label scarcity and representation quality.

C. Ablation Studies

Why Residual Class Variance? We adopt MC and RCV as reliability metrics for pseudo-label selection, grounded in the theoretical decomposition of the CE objective, which shows that reliable predictions must jointly achieve high confidence

TABLE III
CIFAR-10 AND MINI-IMAGENET TOP-1 TEST ACCURACY

Dataset	Method	Backbone	1000 labels	4000 labels	N
CIFAR-10	VAT	WRN 28-2	81.36	88.95	7
	MeanTeacher	WRN 28-2	82.68	89.64	-
	MixMatch	WRN 28-2	92.25	93.76	2
	ReMixMatch	WRN 28-2	94.27	94.86	2
	FixMatch	WRN 28-2	-	95.59	7
	FlexMatch	WRN 28-2	-	95.60	7
	FreeMatch	WRN 28-2	-	95.62	7
	SoftMatch	WRN 28-2	-	95.42	7
	SimPLE	WRN 28-2	94.84	94.95	7
	CoVar	WRN 28-2	94.99	<u>95.60</u>	-
Mini-ImageNet	Fully Supervised	WRN 28-2	-	95.75	-
	Label Propagation	WRN 28-2	-	29.71	-
	MeanTeacher	WRN 28-2	-	27.49	-
	SimPLE	WRN 28-2	-	49.39	7
	CoVar	WRN 28-2	-	51.48	7
	MixMatch	ResNet-18	-	55.47	2
	MixMatch Enhanced	ResNet-18	-	60.50	7
	SimPLE	ResNet-18	-	<u>66.55</u>	7
	CoVar	ResNet-18	-	69.76	7

* Fully supervised baseline using all the labels and simple augmentation (flip-and-crop). N refers to the number of weak augmentations.

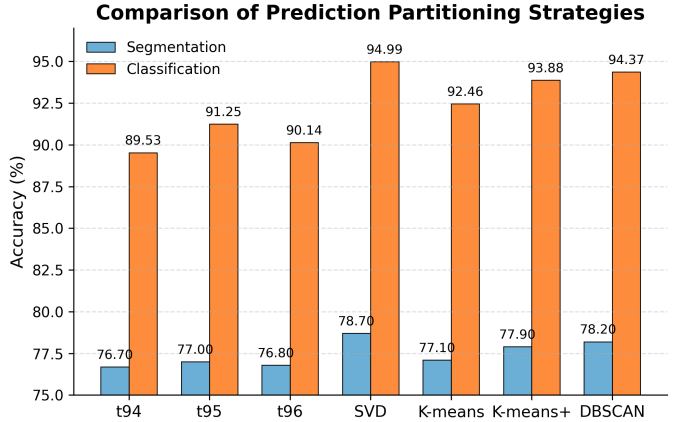


Fig. 7. Ablation studies on different designs of CoVar. Experiments are conducted on the blender PASCAL VOC 2012 (1/8, 321x321) and CIFAR-10 dataset (1000). “t95” means using a fixed confidence threshold of 0.95 to select pseudo labels.

and well-behaved residual-class distributions. In contrast, traditional metrics such as entropy $H(p_j)$, margin m_j , and residual-class entropy H_{res} degenerate under overconfidence, effectively collapsing to comparisons of MC and providing

TABLE IV
COMPARISON OF DIFFERENT COMBINATIONS OF METRICS

v_j	$H(p_j)$	H_{res}	m_j	1/8*	1/4*	1000#	4000#
✓				78.7	79.3	94.99	95.23
✓	✓			77.3	78.5	92.84	93.12
✓		✓		77.5	79.1	94.62	94.88
✓			✓	76.9	78.2	91.10	91.39
✓	✓	✓	✓	71.5	76.3	89.76	90.03
	✓			70.7	72.4	86.45	87.71
		✓		71.6	74.6	88.02	89.28
			✓	69.4	71.9	85.12	86.36

* was conducted in the blender PASCAL VOC 2012 (321x321).

was conducted in the CIFAR-10 dataset.

TABLE V
ABLATION STUDY OF DIFFERENT ε VALUES

ε values	1/8*	1/4*	1000#	4000#
0.1	77.9	78.2	93.20	93.88
0.01	78.1	78.6	93.35	94.00
0.001	77.5	78.0	92.88	93.51
0.0001	77.4	77.8	92.45	93.03
0.00001	77.3	77.6	92.10	92.83
0.000001	77.0	77.5	91.78	92.43
0.0000001	76.9	77.5	91.34	92.02
0.00000001	76.9	77.6	91.05	91.72
$(1 - p_i(k'))/(K - 1)$	78.7	79.3	94.99	95.23

* was conducted in the blender PASCAL VOC 2012 (321x321).

was conducted in the CIFAR-10 dataset.

weak discrimination for multi-modal or uneven residual probabilities. RCV v_j maintains stable scale and sensitivity to residual dispersion, and our ablations show that replacing it with alternative metrics or adding redundant features consistently degrades performance, confirming that the joint use of MC and RCV is a simple yet theoretically justified choice for pseudo-label reliability. As further illustrated in Fig. 6, during training the selected pseudo-labels gradually concentrate around the ideal region near $(p_j(k'), v_j) = (1, 0)$ in the MC-RCV plane, moving from scattered low-quality predictions in early epochs toward tightly clustered high-confidence, low-variance predictions as accuracy improves.

Comparative Analysis of Different Prediction Partitioning Strategies. To evaluate the robustness of our framework across prediction partitioning strategies (distinguishing high- and low-reliability samples), we compared SVD-based clustering with other clustering methods (e.g., K-means, DBSCAN) and feature-space partitioning approaches (e.g., grid-based, Voronoi partitioning) on the augmented PASCAL VOC 2012 and Cityscapes datasets. Experiments were conducted under low-annotation ratios (1/16, 1/8) with consistent hyperparameters (Fig. 7). Across settings, SVD-based clustering consistently outperforms alternative partitioning strategies and exhibits stronger robustness to noise and complex feature distributions, effectively separating reliable pseudo-labels and providing stable gains in label-scarce scenarios.

Comparative Analysis Under Different ε Values. To validate the rationality of setting $\varepsilon = (1 - p_i(k'))/(K - 1)$, we compared this adaptive approach with fixed ε values (1e-8, 1e-6, 1e-4, 0.01, 0.1) on the augmented PASCAL VOC 2012 and Cityscapes datasets under low-annotation ratios (1/16, 1/8), maintaining consistent hyperparameters. Results in Table. V

TABLE VI
COMPARISON OF DIFFERENT TERMS IN EQ. 14 FOR PSEUDO-LABEL SELECTION

MC	$sRCV$	$Cov(g, v)$	1/8*	1/4*	1000#	4000#
✓			77.9	78.5	94.05	94.21
✓	✓		76.5	77.7	91.94	92.22
✓		✓	76.7	78.3	93.63	93.94
✓	✓	✓	78.7	79.3	94.99	95.23
	✓		71.4	73.1	87.32	88.55
	✓	✓	74.6	76.6	89.02	92.28
	✓		73.4	75.8	85.16	91.37

* was conducted in the blender PASCAL VOC 2012 (321x321).

was conducted in the CIFAR-10 dataset.

TABLE VII
ABLATION STUDY OF NONLINEAR WEIGHTING COEFFICIENT $g_j(p_j(k'))$ DESIGNS

$g_j(p_j(k'))$ values	1/8*	1/4*	1000#	4000#
Entropy-Based: $c/H(p_j)$	78.0	78.7	93.45	94.01
Clipped:min(w_o, w_c)	77.6	77.9	92.95	93.33
NoWeight:0	77.2	77.5	92.70	92.23
Linear:1	77.8	78.1	91.82	92.91
Const:10($K - 1$) ²	78.1	78.5	91.95	92.12
Alt-Rational: $\frac{(K-1)^2}{2(1-p_j(k')+\delta)}$	77.9	78.7	92.05	93.72
Full: $\frac{(K-1)^2}{2(1-p_j(k'))}$	78.7	79.3	94.99	95.23

* was conducted in the blender PASCAL VOC 2012 (321x321).

was conducted in the CIFAR-10 dataset.

indicate that the adaptive ε achieves the best performance across all splits. Very small fixed ε (1e-8, 1e-6) incur slight degradations due to numerical issues, while larger ε (0.01, 0.1) lead to more pronounced drops as they deviate from the near-zero assumption. This adaptive setting balances theoretical fidelity and numerical stability, confirming its effectiveness for pseudo-label optimization.

Ablation Study of Nonlinear Weighting Coefficient $g_j(p_j(k'))$. To validate the necessity of the adaptive nonlinear weighting coefficient $g_j(p_j(k')) = \frac{(K-1)^2}{2(1-p_j(k'))}$ introduced in Eq. 16, we systematically compared six alternative designs on the blended PASCAL VOC 2012 (1/8, 1/4 splits) and CIFAR-10 (1000, 4000 labels) datasets, maintaining consistent hyperparameters and backbones across all variants. Results in Table. VII show that the proposed Full formulation consistently achieves the best results, surpassing the strongest alternative by +0.6-0.7 mIoU on VOC and +1.2-1.5 percentage points on CIFAR-10.

Specifically, removing the weighting entirely (NoWeight) results in substantial degradation (-1.5% to -3.0%), confirming that explicit penalization of residual-class variance is essential for reliable pseudo-label selection. Fixed weighting schemes (Const) fail to capture the confidence-dependent dynamics, leading to suboptimal discrimination between high- and moderate-confidence predictions (-0.6% to -3.1%). Linear weighting partially restores discriminative power but lacks the sharp penalty escalation at high confidence levels (-0.9% to -3.2%). The Clipped variant, which caps the maximum weight to avoid numerical instability, also underperforms (-1.1% to -2.0%). This indicates that the unbounded growth of $g_j(p_j(k'))$ as $p_j(k') \rightarrow 1$ is consistent with our CE decomposition

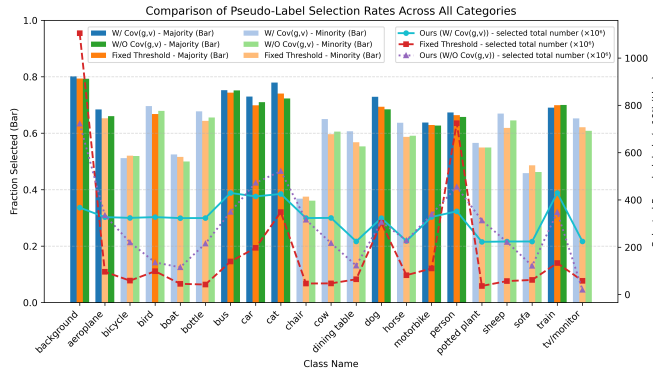


Fig. 8. Class-wise pseudo-label selection rates during training on blended PASCAL VOC 2012 (1/4, 321×321). The fixed-threshold baseline over-selects majority classes and exhibits volatile selection for minority categories. Incorporating $\text{Cov}(g, v)$, CoVar yields smoother trajectories and more balanced selection across classes by coupling high MC with low RCV.

and empirically leads to better performance than bounded alternatives. It enforces stricter uniformity requirements on residual-class distributions for near-certain predictions.

The Alt-Rational design, which introduces a small stabilizing constant δ in the denominator to avoid singularities, achieves competitive results on VOC (within -0.6-0.8 mIoU) but shows degraded performance on CIFAR-10 (-1.5% to -2.9%), suggesting that the singularity at $p_j(k') = 1$ acts as a useful regularizer that should not be overly damped. Interestingly, the Entropy-Based variant $c/H(p_j)$ performs comparably to Full on VOC but falls short on CIFAR-10 (-1.2% to -1.5%), revealing that while prediction entropy correlates with reliability, it conflates information across all classes rather than isolating residual-class dispersion as RCV does. These results validate our theoretical choice to penalize residual-class variance with an adaptive, confidence-dependent coefficient that grows as uncertainty diminishes, thereby enforcing progressively tighter reliability constraints on high-confidence predictions.

Robustness Across Majority and Minority Classes. Fig. 8 visualizes class-wise pseudo-label selection rates during training on the blended PASCAL VOC 2012 (1/4, 321×321). Relative to the fixed-threshold baseline (t95), CoVar demonstrates: (i) balanced coverage across head and tail classes, reducing the gap in selection rates between majority and minority categories; (ii) smoother temporal evolution of selection curves with fewer spikes and oscillations; and (iii) earlier and sustained activation for minority classes, preventing selection starvation in early stages and collapse in later stages. These behaviors arise from the covariance term $\text{Cov}(g, v)$ in our batch objective, which couples maximum confidence (MC) with residual-class variance (RCV). By discouraging cases where high confidence coexists with poor residual-class uniformity, CoVar suppresses overconfident yet unreliable head-class pseudo-labels and reallocates capacity to reliable samples across all classes. The result is a smoother, more equitable selection process than confidence-only rules, yielding robustness under class imbalance.

D. Limitations

Despite its theoretical grounding and empirical gains, CoVar has several limitations. First, when the labeled set is extremely small, the marginal distributions of labeled and unlabeled data can differ substantially. In such cases, even a confidence-variance based criterion cannot fully remove selection bias induced by this distribution shift, and pseudo-label quality may degrade, especially on highly imbalanced or non-stationary datasets.

Second, although our analysis of residual-class dispersion is derived under a general entropy minimization principle, we only instantiate and validate CoVar on semi-supervised semantic segmentation and image classification. Extending the same decomposition and batch-level formulation to related scenarios such as semi-supervised detection and unsupervised domain adaptation may require additional modeling of task-specific architectures, losses, and sampling schemes.

Finally, CoVar relies on masking high-confidence regions to enhance learning in surrounding low-confidence areas. We observe that some masked low-confidence regions become more accurate after context suppression but remain unused due to conservative reliability screening. Designing stable mechanisms to safely recycle such “emergent reliable” predictions is a promising direction to further improve sample efficiency.

V. CONCLUSION

This paper presented CoVar, a unified Confidence-Variance framework for pseudo-label selection in semi-supervised learning. Starting from entropy minimization, we derived a second-order decomposition of cross-entropy that decouples maximum confidence from residual-class variance, yielding a per-sample reliability measure with explicit approximation bounds and a batch-level lower bound involving a confidence-variance covariance term. This analysis shows that reliable pseudo-labels require jointly high confidence and low residual-class dispersion, and motivates an adaptive weighting $g_j(p_j(k'))$ that strengthens variance penalties as confidence increases. Building on this theory, we reformulated pseudo-label selection as a spectral relaxation problem in a confidence-variance feature space and derived an efficient solution that is closely related to kernel spectral clustering. The resulting CoVar module can be plugged into existing semi-supervised pipelines to adaptively separate high- and low-reliability predictions without hand-tuned confidence thresholds. Experiments on PASCAL VOC 2012, Cityscapes, CIFAR-10, and Mini-ImageNet with varied backbones show consistent gains over strong baselines, especially in low-label and imbalanced regimes. Future work will extend CoVar to domain adaptation and other uncertainty-aware settings and integrate it with calibration to further close the gap between reliability theory and large-scale deployment.

REFERENCES

- [1] L. Yang, Z. Zhao, and H. Zhao, “Unimatch v2: Pushing the limit of semi-supervised semantic segmentation,” *IEEE TPAMI*, 2025.
- [2] J. Wu, Z. Li, W. Sun, J. Yin, L. Nie, and Z. Lin, “Clusmatch: Improving deep clustering by unified positive and negative pseudo-label learning,” *IEEE Transactions on Pattern Analysis and Machine Intelligence*, 2025.

[3] E. Tarubinga and J. Kalafatovich Espinoza, “Confidence-weighted boundary-aware learning for semi-supervised semantic segmentation,” *arXiv e-prints*, pp. arXiv–2502, 2025.

[4] H. Li, N. Wang, X. Yang, X. Wang, and X. Gao, “An enhanced adaptive confidence margin for semi-supervised facial expression recognition,” *IEEE Transactions on Pattern Analysis and Machine Intelligence*, 2025.

[5] Q. Xie, Z. Dai, E. Hovy, T. Luong, and Q. Le, “Unsupervised data augmentation for consistency training,” *NeurIPS*, vol. 33, pp. 6256–6268, 2020.

[6] J. Kim, Y. Min, D. Kim, G. Lee, J. Seo, K. Ryoo, and S. Kim, “Comatch: Semi-supervised learning with confidence-guided consistency regularization,” in *ECCV*. Springer, 2022, pp. 674–690.

[7] Y. Wang, H. Chen, Y. Fan, W. Sun, R. Tao, W. Hou, R. Wang, L. Yang, Z. Zhou, L.-Z. Guo *et al.*, “Usb: A unified semi-supervised learning benchmark for classification,” *NeurIPS*, vol. 35, pp. 3938–3961, 2022.

[8] P. Liu and J. Liu, “When confidence fails: Revisiting pseudo-label selection in semi-supervised semantic segmentation,” in *ICCV*, October 2025, pp. 21 874–21 884.

[9] Q. Xie, M.-T. Luong, E. Hovy, and Q. V. Le, “Self-training with noisy student improves imagenet classification,” in *CVPR*, 2020, pp. 10 687–10 698.

[10] B. Zoph, G. Ghiasi, T.-Y. Lin, Y. Cui, H. Liu, E. D. Cubuk, and Q. Le, “Rethinking pre-training and self-training,” *NeurIPS*, vol. 33, pp. 3833–3845, 2020.

[11] J. Liu, Z. Jiang, W. Gui, Z. Chen, and C. Zhang, “Occlusion segmentation: Restore and segment invisible areas for particle objects,” *IEEE TASE*, 2024.

[12] A. Tarvainen and H. Valpola, “Mean teachers are better role models: Weight-averaged consistency targets improve semi-supervised deep learning results,” *NeurIPS*, vol. 30, 2017.

[13] K. Sohn, D. Berthelot, N. Carlini, Z. Zhang, H. Zhang, C. A. Raffel, E. D. Cubuk, A. Kurakin, and C.-L. Li, “Fixmatch: Simplifying semi-supervised learning with consistency and confidence,” *NeurIPS*, vol. 33, pp. 596–608, 2020.

[14] B. Zhang, Y. Wang, W. Hou, H. Wu, J. Wang, M. Okumura, and T. Shinozaki, “Flexmatch: Boosting semi-supervised learning with curriculum pseudo labeling,” *NeurIPS*, vol. 34, pp. 18 408–18 419, 2021.

[15] Y. Wang, H. Chen, Q. Heng, W. Hou, Y. Fan, Z. Wu, J. Wang, M. Savvides, T. Shinozaki, B. Raj *et al.*, “Freematch: Self-adaptive thresholding for semi-supervised learning,” in *ICLR*, 2023.

[16] H. Chen, R. Tao, Y. Fan, Y. Wang, J. Wang, B. Schiele, X. Xie, B. Raj, and M. Savvides, “Softmatch: Addressing the quantity-quality tradeoff in semi-supervised learning,” in *ICLR*, 2023.

[17] C. Guo, G. Pleiss, Y. Sun, and K. Q. Weinberger, “On calibration of modern neural networks,” in *Proceedings of the 34th International Conference on Machine Learning (ICML)*. PMLR, 2017, pp. 1321–1330.

[18] J. C. Platt, “Probabilistic outputs for support vector machines and comparisons to regularized likelihood methods,” *Advances in large margin classifiers*, vol. 10, no. 3, pp. 61–74, 1999.

[19] B. Zadrozny and C. Elkan, “Obtaining calibrated probability estimates from decision trees and naive bayesian classifiers,” in *Proceedings of the 18th International Conference on Machine Learning (ICML)*. Morgan Kaufmann, 2001, pp. 609–616.

[20] C. Szegedy, V. Vanhoucke, S. Ioffe, J. Shlens, and Z. Wojna, “Rethinking the inception architecture for computer vision,” in *Proceedings of the IEEE Conference on Computer Vision and Pattern Recognition (CVPR)*, 2016, pp. 2818–2826.

[21] T.-Y. Lin, P. Goyal, R. Girshick, K. He, P. Dollár *et al.*, “Focal loss for dense object detection,” in *Proceedings of the IEEE International Conference on Computer Vision (ICCV)*, 2017, pp. 2980–2988.

[22] H. Zhang, M. Cisse, Y. N. Dauphin, and D. Lopez-Paz, “mixup: Beyond empirical risk minimization,” in *International Conference on Learning Representations (ICLR)*, 2018.

[23] S. Yun, D. Han, S. Chun, S. J. Oh, Y. Yoo, and J. Choe, “Cutmix: Regularization strategy to train strong classifiers with localizable features,” in *Proceedings of the IEEE International Conference on Computer Vision (ICCV)*, 2019, pp. 6023–6032.

[24] M. N. Rizve, K. Duarte, Y. S. Rawat, and M. Shah, “In defense of pseudo-labeling: An uncertainty-aware pseudo-label selection framework for semi-supervised learning,” *arXiv preprint arXiv:2101.06329*, 2021.

[25] K. Wang, Y. Nie, C. Fang, C. Han, X. Wu, X. Wang, L. Lin, F. Zhou, and G. Li, “Double-check soft teacher for semi-supervised object detection,” in *IJCAI*, 2022, pp. 1430–1436.

[26] S. Li, W. Jin, Z. Wang, F. Wu, Z. Liu, C. Tan, and S. Z. Li, “Semireward: A general reward model for semi-supervised learning,” in *ICLR*, 2024.

[27] Z. Wang, Z. Chen, C. Liu, Y. Zhao, X. Zhu, and Q. J. Wu, “Diversity augmentation and multi-fuzzy label for semi-supervised semantic segmentation,” *Neurocomputing*, p. 129681, 2025.

[28] Y. Liu, Y. Tian, Y. Chen, F. Liu, V. Belagiannis, and G. Carneiro, “Perturbed and strict mean teachers for semi-supervised semantic segmentation,” in *CVPR*, 2022, pp. 4258–4267.

[29] L. Yang, L. Qi, L. Feng, W. Zhang, and Y. Shi, “Revisiting weak-to-strong consistency in semi-supervised semantic segmentation,” in *CVPR*, 2023, pp. 7236–7246.

[30] J. Liu, Z. Jiang, T. Cao, Z. Chen, C. Zhang, and W. Gui, “Generated pseudo-labels guided by background skeletons for overcoming under-segmentation in overlapping particle objects,” *TCSVT*, vol. 33, no. 6, pp. 2906–2919, 2022.

[31] H. Hu, F. Wei, H. Hu, Q. Ye, J. Cui, and L. Wang, “Semi-supervised semantic segmentation via adaptive equalization learning,” *NeurIPS*, vol. 34, pp. 22 106–22 118, 2021.

[32] R. Sun, H. Mai, T. Zhang, and F. Wu, “Daw: exploring the better weighting function for semi-supervised semantic segmentation,” *NeurIPS*, vol. 36, 2024.

[33] J. Ma, C. Wang, Y. Liu, L. Lin, and G. Li, “Enhanced soft label for semi-supervised semantic segmentation,” in *CVPR*, 2023, pp. 1185–1195.

[34] Y. Wang, H. Wang, Y. Shen, J. Fei, W. Li, G. Jin, L. Wu, R. Zhao, and X. Le, “Semi-supervised semantic segmentation using unreliable pseudo-labels,” in *CVPR*, 2022, pp. 4248–4257.

[35] B. Sun, Y. Yang, L. Zhang, M.-M. Cheng, and Q. Hou, “Corrmatch: Label propagation via correlation matching for semi-supervised semantic segmentation,” in *CVPR*, 2024, pp. 3097–3107.

[36] X. Wang, M. Long, J. Wang, and M. Jordan, “Transferable calibration with lower bias and variance in domain adaptation,” *Advances in Neural Information Processing Systems*, vol. 33, pp. 19 212–19 223, 2020.

[37] L. Hoyer, D. Dai, H. Wang, and L. Van Gool, “Mic: Masked image consistency for context-enhanced domain adaptation,” in *CVPR*, 2023, pp. 11 721–11 732.

[38] S. Thulasidasan, G. Chennupati, J. A. Bilmes, T. Bhattacharya, and S. Michalak, “On mixup training: Improved calibration and predictive uncertainty for deep neural networks,” *Advances in neural information processing systems*, vol. 32, 2019.

[39] V. Verma, K. Kawaguchi, A. Lamb, J. Kannala, A. Solin, Y. Bengio, and D. Lopez-Paz, “Interpolation consistency training for semi-supervised learning,” *Neural Networks*, vol. 145, pp. 90–106, 2022.

[40] C. Olsson, A. P. Eriksson, and F. Kahl, “Improved spectral relaxation methods for binary quadratic optimization problems,” *Computer Vision and Image Understanding*, vol. 112, no. 1, pp. 3–13, 2008.

[41] G. Tian, “Generalized kkm theorems, minimax inequalities, and their applications,” *Journal of Optimization Theory and Applications*, vol. 83, pp. 375–389, 1994.

[42] M. Everingham, S. A. Eslami, L. Van Gool, C. K. Williams, J. Winn, and A. Zisserman, “The pascal visual object classes challenge: A retrospective,” *IJCV*, vol. 111, pp. 98–136, 2015.

[43] M. Cordts, M. Omran, S. Ramos, T. Rehfeld, M. Enzweiler, R. Benenson, U. Franke, S. Roth, and B. Schiele, “The cityscapes dataset for semantic urban scene understanding,” in *CVPR*, 2016, pp. 3213–3223.

[44] B. Hariharan, P. Arbeláez, L. Bourdev, S. Maji, and J. Malik, “Semantic contours from inverse detectors,” in *ICCV*, 2011, pp. 991–998.

[45] A. Krizhevsky, G. Hinton *et al.*, “Learning multiple layers of features from tiny images,” 2009.

[46] O. Vinyals, C. Blundell, T. Lillicrap, D. Wierstra *et al.*, “Matching networks for one shot learning,” *Advances in neural information processing systems*, vol. 29, 2016.

[47] L. Yang, W. Zhuo, L. Qi, Y. Shi, and Y. Gao, “St++: Make self-training work better for semi-supervised semantic segmentation,” in *CVPR*, 2022, pp. 4258–4267.

[48] X. Lai, Z. Tian, L. Jiang, S. Liu, H. Zhao, L. Wang, and J. Jia, “Semi-supervised semantic segmentation with directional context-aware consistency,” in *CVPR*, 2021, pp. 1205–1214.

[49] S. Li, Y. He, W. Zhang, W. Zhang, X. Tan, J. Han, E. Ding, and J. Wang, “Cfcg: Semi-supervised semantic segmentation via cross-fusion and contour guidance supervision,” in *CVPR*, 2023, pp. 16 348–16 358.

[50] Z. Wang, Z. Zhao, X. Xing, D. Xu, X. Kong, and L. Zhou, “Conflict-based cross-view consistency for semi-supervised semantic segmentation,” in *CVPR*, 2023, pp. 19 585–19 595.

[51] P. Li, P. Purkait, T. Ajanthan, M. Abdolshah, R. Garg, H. Husain, C. Xu, S. Gould, W. Ouyang, and A. Van Den Hengel, “Semi-supervised semantic segmentation under label noise via diverse learning groups,” in *CVPR*, 2023, pp. 1229–1238.

- [52] H. Mai, R. Sun, T. Zhang, and F. Wu, “Rankmatch: Exploring the better consistency regularization for semi-supervised semantic segmentation,” in *CVPR*, 2024, pp. 3391–3401.
- [53] X. Wang, B. Zhang, L. Yu, and J. Xiao, “Hunting sparsity: Density-guided contrastive learning for semi-supervised semantic segmentation,” in *CVPR*, 2023, pp. 3114–3123.
- [54] H. Wang, Q. Zhang, Y. Li, and X. Li, “Allspark: Reborn labeled features from unlabeled in transformer for semi-supervised semantic segmentation,” in *CVPR*, 2024, pp. 3627–3636.
- [55] X. Wang, H. Bai, L. Yu, Y. Zhao, and J. Xiao, “Towards the uncharted: Density-descending feature perturbation for semi-supervised semantic segmentation,” in *CVPR*, 2024, pp. 3303–3312.
- [56] Y. Jin, J. Wang, and D. Lin, “Semi-supervised semantic segmentation via gentle teaching assistant,” *NeurIPS*, vol. 35, pp. 2803–2816, 2022.
- [57] Z. Zhao, L. Yang, S. Long, J. Pi, L. Zhou, and J. Wang, “Augmentation matters: A simple-yet-effective approach to semi-supervised semantic segmentation,” in *CVPR*, 2023, pp. 11350–11359.
- [58] X. Chen, Y. Yuan, G. Zeng, and J. Wang, “Semi-supervised semantic segmentation with cross pseudo supervision,” in *CVPR*, 2021, pp. 2613–2622.
- [59] L. Hoyer, D. J. Tan, M. F. Naeem, L. Van Gool, and F. Tombari, “Semivl: semi-supervised semantic segmentation with vision-language guidance,” in *European Conference on Computer Vision*. Springer, 2024, pp. 257–275.
- [60] P. Qiao, Z. Wei, Y. Wang, Z. Wang, G. Song, F. Xu, X. Ji, C. Liu, and J. Chen, “Fuzzy positive learning for semi-supervised semantic segmentation,” in *CVPR*, 2023, pp. 15465–15474.
- [61] L.-C. Chen, Y. Zhu, G. Papandreou, F. Schroff, and H. Adam, “Encoder-decoder with atrous separable convolution for semantic image segmentation,” in *ECCV*, 2018, pp. 801–818.
- [62] K. He, X. Zhang, S. Ren, and J. Sun, “Deep residual learning for image recognition,” in *CVPR*, 2016, pp. 770–778.

Supplementary Material

I. OVERVIEW

In the supplementary material for CoVar, we provide a proof of Eq. (9)-(14), (17) (Sec.II-A), give a low-complexity implementation of CoVar and pseudo-code (Sec.III), extend the implementation details and experimental comparison (Sec.IV).

II. PROOF OF EQUATION (9)-(14), (17)

A. Proof of Equation (9)-(14)

Validity of the Taylor approximation and error bounds. We now make explicit the regularity conditions under which the second-order expansion in Eq. (9)-(10) is valid and quantitatively accurate.

Assumption 1 (Residual-scale boundedness). *For each sample j and every non-maximum class $k \neq k'$, let $\mu_j = \frac{1-p_j(k')}{K-1}$ and $\delta_j(k) = p_j(k) - \mu_j$ with $\sum_{k \neq k'} \delta_j(k) = 0$. Assume there exists $\rho \in (0, 1)$ such that $|\delta_j(k)| \leq \rho \mu_j$ for all $k \neq k'$. Equivalently, all residual-class probabilities satisfy $p_j(k) \in [(1-\rho)\mu_j, (1+\rho)\mu_j] \subset (0, 1)$.*

Under Assumption 1, $\mu_j - |\delta_j(k)| > 0$ and the Lagrange form of the Taylor remainder for $\log x$ yields a uniform cubic bound.

Lemma 1 (Quadratic CE decomposition with bounded remainder). *Let $f(x) = \log x$ and suppose Assumption 1 holds. Then for every $k \neq k'$ there exists $\xi_{jk} \in ((1-\rho)\mu_j, (1+\rho)\mu_j)$ such that*

$$\log p_j(k) = \log \mu_j + \frac{\delta_j(k)}{\mu_j} - \frac{\delta_j^2(k)}{2\mu_j^2} + R_2(p_j(k)), \quad (1)$$

with $|R_2(p_j(k))| \leq \frac{|\delta_j(k)|^3}{3\xi_{jk}^3} \leq \frac{|\delta_j(k)|^3}{3(1-\rho)^3 \mu_j^3}$.

Consequently, substituting into Eq. (9) gives the per-sample cross-entropy decomposition

$$CE(p_j, q_j) = -f_j(p_j(k')) + g_j(p_j(k')) v_j + R_j, \quad (2)$$

where $v_j = \frac{1}{K-1} \sum_{k \neq k'} \delta_j^2(k)$, f_j and g_j are as in Eq. (11), and the remainder is bounded by

$$|R_j| \leq C_j v_j^{3/2}, \quad C_j \triangleq \frac{(K-1)^{3/2} \varepsilon}{3(1-\rho)^3 \mu_j^3}. \quad (3)$$

Moreover, $f_j(p_j(k'))$ and $g_j(p_j(k'))$ are strictly increasing in $p_j(k') \in (0, 1)$.

Proof sketch. The bound follows from the third derivative $f^{(3)}(x) = 2/x^3$ and the Lagrange remainder of order three, together with $\sum_{k \neq k'} \delta_j(k) = 0$ and the inequality $\sum_{k \neq k'} |\delta_j(k)|^3 \leq (K-1)^{3/2} v_j^{3/2}$.

Theorem 1 (Joint reliability criterion and boundary behavior). *Suppose Assumption 1 holds for a fixed sample j and let $\varepsilon > 0$. Then:*

- (i) *For fixed total residual mass $1-p_j(k')$ (equivalently fixed $\mu_j > 0$), $CE(p_j, q_j)$ is minimized when the residual-class probabilities are uniform, i.e., $v_j = 0$.*
- (ii) *For fixed $v_j > 0$, $CE(p_j, q_j)$ is strictly decreasing in $p_j(k')$, and the marginal penalty weight on v_j equals $g_j(p_j(k')) = \frac{(K-1)^3 \varepsilon}{2(1-p_j(k'))^2}$, which is strictly increasing in $p_j(k')$. In particular, for any $\gamma \in (0, 1)$, if $p_j(k') \leq 1 - \gamma$ then $g_j(p_j(k')) \leq \frac{(K-1)^3 \varepsilon}{2\gamma^2}$, whereas as $p_j(k') \rightarrow 1$, $g_j(p_j(k')) \rightarrow \infty$ at rate $\Theta((1-p_j(k'))^{-2})$.*
- (iii) *Consequently, a prediction is reliable only if it jointly achieves large $p_j(k')$ and small v_j ; relying on $p_j(k')$ alone is insufficient when v_j is large. The approximation error satisfies $|R_j| \leq C_j v_j^{3/2}$ with C_j as in Lemma 1.*

Proof sketch. (i) follows from Jensen's inequality applied to $-\log(\cdot)$ under the constraint $\sum_{k \neq k'} p_j(k) = 1 - p_j(k')$. (ii) follows from the monotonicity of f_j and g_j in $p_j(k')$. (iii) combines (i)–(ii) with Lemma 1.

Corollary 1 (Single-sample reliability with $\varepsilon = \mu_j$). *Under Assumption 1 and the adaptive setting $\varepsilon = \mu_j = \frac{1-p_j(k')}{K-1}$, the per-sample cross-entropy admits the decomposition*

$$CE(p_j, q_j) = -\log p_j(k') + \frac{(K-1)^2}{2(1-p_j(k'))} v_j + R_j,$$

with remainder bounded as $|R_j| \leq C'_j v_j^{3/2}$, where $C'_j = \frac{(K-1)^{3/2}}{3(1-\rho)^3 \mu_j^2}$. Moreover:

- (i) *For fixed residual mass $1 - p_j(k')$, the minimum is attained at uniform residuals $v_j = 0$.*
- (ii) *For fixed $v_j > 0$, the penalty weight on v_j equals $\frac{(K-1)^2}{2(1-p_j(k'))}$, which is strictly increasing in $p_j(k')$, is bounded by $\frac{(K-1)^2}{2\gamma}$ whenever $p_j(k') \leq 1 - \gamma$, and diverges as $p_j(k') \rightarrow 1$ at rate $\Theta((1-p_j(k'))^{-1})$.*

Consequently, under $\varepsilon = \mu_j$, reliable predictions require jointly large $p_j(k')$ and small v_j , with an adaptively stronger dispersion penalty as confidence increases.

Proof sketch. Substitute $\varepsilon = \mu_j$ into Theorem 1 and Lemma 1 to obtain the simplified coefficient and remainder constant.

Theorem 2 (Batch-level lower bound and adaptive weighting). *Under Assumption 1 and with the adaptive choice $\varepsilon = \mu_j = \frac{1-p_j(k')}{K-1}$ for each prediction, the batch cross-entropy satisfies the lower bound in Eq. (14) up to a remainder*

$$R_B \triangleq \frac{1}{N_B} \sum_{j=1}^{N_B} R_j, \quad \text{with} \quad |R_B| \leq \frac{1}{N_B} \sum_{j=1}^{N_B} C_j v_j^{3/2},$$

where C_j is given in Lemma 1. Moreover, the coefficient on v_j equals $\frac{(K-1)^2}{2(1-p_j(k'))}$, which is strictly increasing in $p_j(k')$ and thus imposes stronger dispersion penalization on higher-confidence predictions.

Proof sketch. Substitute Lemma 1 into the batch average and use $\varepsilon = \mu_j$ to simplify terms; the bound follows by averaging the per-sample remainders.

B. Proof of Equation (17)

For the pseudo-label selection problem in semi-supervised semantic segmentation, it can be formulated as:

$$\max_S \text{Tr}(S^T \Phi^T \Phi S), \text{ s.t. } S \in \{0, 1\}^{N \times 2},$$

where S is the binary selection matrix subject to $\sum_c S_{n,c} = 1$ with $c \in \{1, 2\}$ indicating class indices, and $\text{Tr}(\cdot)$ denotes the matrix trace. Each column of $\Phi = [\mathbf{h}_1, \mathbf{h}_2, \dots, \mathbf{h}_N]$ represents the feature $\mathbf{h}_n \in \mathbb{R}^2$ of pixel n .

Proof. Without loss of generality, the essential goal of pseudo-label selection is to assign pixel classes via S such that the selected pseudo-labels are optimal under a certain metric:

$$\mathcal{L}(S) = \sum_{n=1}^{HW} \varphi(\mathbf{z}_n, S_{n,:}),$$

where $\varphi(\cdot, \cdot)$ is a function that measures the potential risk of assigning pixel n to a specific class, with \mathbf{z}_n representing the pixel's feature. Considering the potential natural separation exhibited in 1, we employ intra-class consistency as the metric, which measures the distance between the pixel feature vector $\mathbf{z}_n = \mathbf{h}_n$ and the mean feature vector μ_c of its assigned class c , which can be expressed as

$$\varphi(\mathbf{z}_n, S_{n,:}) = \sum_{c=1}^2 S_{n,c} \|\mathbf{h}_n(c) - \mu_c\|^2,$$

thus $\mathcal{L}(S)$ can be reformulated as

$$\mathcal{L}(S) = \|\Phi - S(S^T S)^{-1} S^T \Phi\|_F^2,$$

let $\mathbf{P} = S(S^T S)^{-1} S^T$, the $\mathcal{L}(S)$ simplifies to

$$\mathcal{L}(S) = \|\Phi - \mathbf{P}\Phi\|_F^2.$$

Using the Frobenius norm identity

$$\mathcal{L}(S) = \|\Phi\|_F^2 - 2 \text{Tr}(\Phi^T \mathbf{P}\Phi) + \|\mathbf{P}\Phi\|_F^2,$$

since $\mathbf{P}^2 = \mathbf{P}$ (idempotence of projection matrices), thus

$$\mathcal{L}(S) = \|\Phi\|_F^2 - \text{Tr}(\Phi^T \mathbf{P}\Phi).$$

Minimizing $\mathcal{L}(S)$ is equivalent to maximizing $\text{Tr}(\Phi^T \mathbf{P}\Phi)$. Substituting \mathbf{P} :

$$\text{Tr}(\Phi^T \mathbf{P}\Phi) = \text{Tr}(\Phi^T S(S^T S)^{-1} S^T \Phi),$$

for binary classification, $S^T S = \text{diag}(n_1, n_2)$, where n_1 and n_2 are the number of pixels in each class. Thus:

$$\text{Tr}(\Phi^T \mathbf{P}\Phi) = \text{Tr}(S^T \Phi \Phi^T S) \cdot (n_1^{-1} + n_2^{-1}),$$

ignoring the normalization constant, this reduces to:

$$\max_S \text{Tr}(S^T \Phi^T \Phi S).$$

III. ALGORITHM

A. Low-complexity Implementation of Prediction Convex Optimization Separation

In Eq. (17), we used the eigenvectors u_i of $\Phi^T \Phi$. However, obtaining u_i through $\Phi^T \Phi$ is computationally expensive, especially when $\Phi \in \mathbb{R}^{2 \times HW}$ has a large number of columns, where $HW \gg 2$ (segmentation tasks). So we provide an efficient alternative with Singular Value Decomposition (SVD).

The SVD of Φ is given by:

$$\Phi = \mathbf{U} \Sigma \mathbf{V}^T,$$

where $\mathbf{U} \in \mathbb{R}^{2 \times 2}$ and $\mathbf{V} \in \mathbb{R}^{HW \times HW}$ are orthogonal matrix, $\Sigma \in \mathbb{R}^{2 \times HW}$ is a diagonal matrix containing the singular values σ_i .

Substituting the SVD of Φ ,

$$\Phi^T \Phi = (\mathbf{U} \Sigma \mathbf{V}^T)^T (\mathbf{U} \Sigma \mathbf{V}^T),$$

which simplifies to

$$\Phi^T \Phi = \mathbf{V} \Sigma^T \mathbf{U}^T \mathbf{U} \Sigma \mathbf{V}^T.$$

Using the orthogonality of \mathbf{U} ($\mathbf{U}^T \mathbf{U} = \mathbf{I}$),

$$\Phi^T \Phi = \mathbf{V} \Sigma^T \Sigma \mathbf{V}^T.$$

Let $\Lambda = \Sigma^T \Sigma = \text{diag}(\sigma_1^2, \sigma_2^2)$, where σ_i^2 are the squared singular values. Then

$$\Phi^T \Phi = \mathbf{V} \Lambda \mathbf{V}^T.$$

This shows that \mathbf{V} contains the eigenvectors of $\Phi^T \Phi$, Λ contains the eigenvalues of $\Phi^T \Phi$.

Computing the eigenvectors of $\Phi^T \Phi$ via direct eigen-decomposition requires explicitly forming $\Phi^T \Phi$, which has a cost of $\mathcal{O}(2(HW)^2)$ for matrix multiplication and $\mathcal{O}(HW^3)$ for eigen-decomposition. In contrast, computing the SVD of Φ has a cost of $\mathcal{O}(2(HW)^2)$.

B. Pseudocode for Optimization Separation

Algorithm 1 provides the pseudocode for Prediction Convex Optimization Separation. Using a convex optimization strategy based on confidence distribution, CoVar effectively excludes a large number of high-confidence false predictions in pseudo-label selection to improve the performance in semi-supervised semantic segmentation tasks.

IV. EXTENSIVE EXPERIMENT DETAILS

A. More Implementation Details

Following prior works [1], we employ random scaling between [0.5, 2.0], cropping, and flipping as weak augmentations. We combine ColorJitter, random grayscale, Gaussian blur, and CutMix [2] for strong augmentations. Weak augmentations and a modified strong augmentation (without random grayscale and Gaussian blur) are applied. Additionally, we incorporate 50% random channel dropout as feature perturbations to encourage robust feature representations as in previous works [3]. For computational efficiency, mixed-precision training based on BrainFloat16 is utilized.

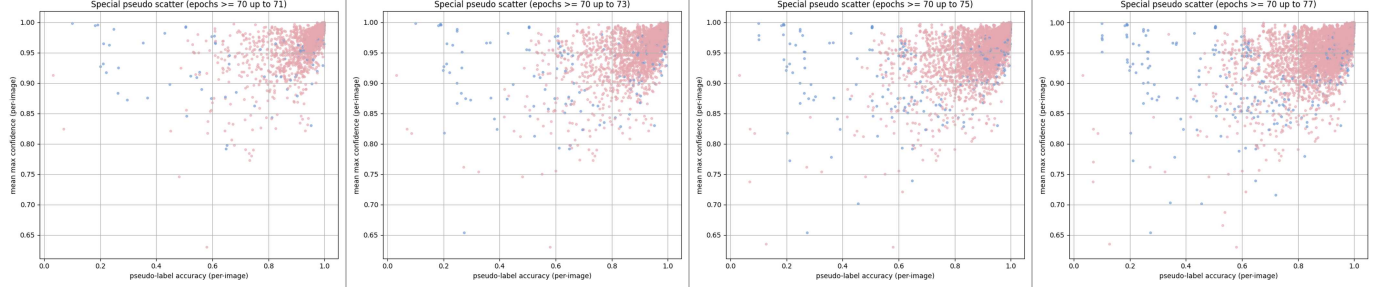


Fig. 1. Evolution of pseudo-label selection during training on PASCAL VOC 2012 (1/8, 513×513). Each scatter plot shows maximum confidence vs. average pseudo-label accuracy at different epochs. Majority-class samples (warmer colors) initially dominate high-confidence regions, while minority-class samples (cooler colors) progressively converge to the high-accuracy quadrant as CoVar’s joint MC-RCV criterion refines selection, achieving balanced coverage by epoch 77.

Algorithm 1 Pseudocode of Prediction Convex Optimization Separation in a PyTorch-like style.

```

1: function PCOS( $p_{max}$ ,  $v_j$ ) #  $p_{max}$ : Maximum Confidence;  $v_j$ : Residual-Class Variance;
 $p_{max}, v_j \in \mathbb{R}^N$ ;  $\Phi \in \mathbb{R}^{2 \times N}$ 
2:   # Combine  $p_{max}$  and  $v_j$  into a feature matrix  $\Phi$ 
3:    $\Phi = \text{stack}([p_{max}, v_j], \text{axis} = 1). \text{T}$ 
4:   # Compute the right singular vectors of  $\Phi$ , which coincide with the eigenvectors of  $\Phi^T \Phi$ 
5:    $U, \Sigma, V^T = \text{svd}(\Phi)$ 
6:    $eig\_vectors = V^T[:, :2]$ 
7:   # Construct the optimal selection matrix
8:    $S = \text{argmax}(\text{abs}(eig\_vectors), \text{axis} = 1)$ 
9:   # Calculate mean and std of each cluster
10:   $stats = []$ 
11:  for  $c$  in  $\{0, 1\}$  do
12:     $\Phi_c = \Phi[:, S == c]$ 
13:     $\mu_c = \Phi_c.\text{mean}(\text{dim} = 1)$ 
14:     $\sigma_c = \Phi_c.\text{std}(\text{dim} = 1)$ 
15:     $stats.append((\mu_c, \sigma_c))$ 
16:  end for
17:  # Select reliable class by a joint criterion
18:   $\lambda = 0.25$  # hyperparameter
19:   $scores = []$ 
20:  for  $(\mu_c, \sigma_c)$  in  $stats$  do
21:     $score_c = \mu_c[0] - \lambda \cdot \sigma_c[1]$ 
22:     $scores.append(score_c)$ 
23:  end for
24:   $c^* = \text{argmax}(scores)$  # index
25:   $(\mu, \sigma) = stats[c^*]$ 
26:  # Smooth loss weight
27:   $weight = \exp\left(-\left(\frac{\Phi - \mu}{2\sigma}\right)^2\right)$ 
28:   $weight = weight.\text{prod}(\text{dim} = 0)$ 
29:  # Preserve clearly reliable predictions
30:   $weight[(\Phi[0, :] > \mu[0]) \& (\Phi[1, :] < \mu[1])] = 1$ 
31:  return  $weight$ 
32: end function

```

B. More Experimental Results

Fig. 1 visualizes pseudo-label selection evolution during training on PASCAL VOC 2012 (1/8, 513×513), plotting maximum confidence (MC) versus average accuracy across epochs 70–77. The figure shows three temporal patterns: (i) early-stage separation, where majority-class samples (warmer colors) dominate high-MC regions while minority-class samples (cooler colors) remain dispersed; (ii) progressive convergence, where minority-class samples shift toward the high-MC/high-accuracy quadrant as CoVar’s joint MC-RCV criterion identifies reliable tail-class samples; and (iii) stabilization, where both classes converge with reduced dispersion. This validates that Cov(g, v) suppresses overconfident yet unreliable predictions, enabling smoother and more equitable selection than fixed-threshold baselines.

C. More Visualizations

Fig. 2 compares qualitative segmentation results on PASCAL VOC 2012 (1/8, 513×513) between UniMatch V1 baseline (W/O CoVar) and our method (With CoVar). CoVar yields three consistent improvements: (i) sharper object boundaries, where the baseline produces blurred or fragmented edges around fine structures (limbs, wheels) while CoVar achieves crisper delineations; (ii) reduced false positives, where the baseline hallucinates spurious regions while CoVar suppresses these artifacts; and (iii) improved tail-class completeness, where the baseline under-segments or misses rare objects (bicycles, potted plants) while CoVar restores coverage. These gains corroborate the quantitative mIoU improvements by enforcing joint MC-RCV reliability.

REFERENCES

- [1] L. Yang, L. Qi, L. Feng, W. Zhang, and Y. Shi, “Revisiting weak-to-strong consistency in semi-supervised semantic segmentation,” in *CVPR*, 2023, pp. 7236–7246.
- [2] S. Yun, D. Han, S. Chun, S. J. Oh, Y. Yoo, and J. Choe, “Cutmix: Regularization strategy to train strong classifiers with localizable features,” in *ICCV*, 2019, pp. 6022–6031.
- [3] B. Sun, Y. Yang, L. Zhang, M.-M. Cheng, and Q. Hou, “Corrmatch: Label propagation via correlation matching for semi-supervised semantic segmentation,” in *CVPR*, 2024, pp. 3097–3107.



Fig. 2. Qualitative comparison of segmentation results on PASCAL VOC 2012 (1/8, 513×513). Top rows show input images and ground truth; middle rows show UniMatch V1 baseline (W/O CoVar); bottom rows show our method (With CoVar). CoVar yields sharper boundaries, reduced false positives, and improved completeness for minority classes compared to the baseline.